

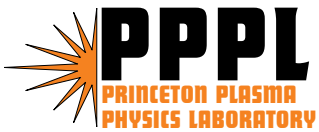
PPPL-4048

PPPL-4048

EBW-bootstrap Current Synergy in the National Spherical Torus Experiment (NSTX)

R.W. Harvey and G. Taylor

February 2005



Prepared for the U.S. Department of Energy under Contract DE-AC02-76CH03073.

PPPL Report Disclaimers

Full Legal Disclaimer

This report was prepared as an account of work sponsored by an agency of the United States Government. Neither the United States Government nor any agency thereof, nor any of their employees, nor any of their contractors, subcontractors or their employees, makes any warranty, express or implied, or assumes any legal liability or responsibility for the accuracy, completeness, or any third party's use or the results of such use of any information, apparatus, product, or process disclosed, or represents that its use would not infringe privately owned rights. Reference herein to any specific commercial product, process, or service by trade name, trademark, manufacturer, or otherwise, does not necessarily constitute or imply its endorsement, recommendation, or favoring by the United States Government or any agency thereof or its contractors or subcontractors. The views and opinions of authors expressed herein do not necessarily state or reflect those of the United States Government or any agency thereof.

Trademark Disclaimer

Reference herein to any specific commercial product, process, or service by trade name, trademark, manufacturer, or otherwise, does not necessarily constitute or imply its endorsement, recommendation, or favoring by the United States Government or any agency thereof or its contractors or subcontractors.

PPPL Report Availability

This report is posted on the U.S. Department of Energy's Princeton Plasma Physics Laboratory Publications and Reports web site in Fiscal Year 2005. The home page for PPPL Reports and Publications is: http://www.pppl.gov/pub_report/

Office of Scientific and Technical Information (OSTI):

Available electronically at: <http://www.osti.gov/bridge>.

Available for a processing fee to U.S. Department of Energy and its contractors, in paper from:

U.S. Department of Energy
Office of Scientific and Technical Information
P.O. Box 62
Oak Ridge, TN 37831-0062
Telephone: (865) 576-8401
Fax: (865) 576-5728
E-mail: reports@adonis.osti.gov

National Technical Information Service (NTIS):

This report is available for sale to the general public from:

U.S. Department of Commerce
National Technical Information Service
5285 Port Royal Road
Springfield, VA 22161
Telephone: (800) 553-6847
Fax: (703) 605-6900
Email: orders@ntis.fedworld.gov
Online ordering: <http://www.ntis.gov/ordering.htm>

EBW-Bootstrap Current Synergy in the National Spherical Torus Experiment (NSTX)

R.W. Harvey

CompX, Del Mar, CA 92014, USA

G. Taylor

Princeton Plasma Physics Laboratory, Princeton, New Jersey 08543, USA

Abstract

Current driven by electron Bernstein waves (EBW) and by the electron bootstrap effect are calculated separately and concurrently with a kinetic code, to determine the degree of synergy between them. A target $\beta = 40\%$ NSTX plasma is examined. A simple bootstrap model in the CQL3D Fokker-Planck code is used in these studies: the transiting electron distributions are connected in velocity-space at the trapped-passing boundary to trapped-electron distributions which are displaced radially by a half-banana width outwards/inwards for the co-/counter-passing regions. This model agrees well with standard bootstrap current calculations, over the outer 60% of the plasma radius. Relatively small synergy net bootstrap current is obtained for EBW power up to 4 MW. Locally, bootstrap current density increases in proportion to increased plasma pressure, and this effect can significantly affect the radial profile of driven current.

PACS# 52.55.Fa, 52.35.Hr

1. Introduction

Modeling of Electron Bernstein wave (EBW) interactions with electrons in the NSTX device shows that the strength of the quasilinear (QL) velocity space diffusion coefficient peaks near the trapped-passing boundary [1]. This result is obtained for second or third harmonic damping towards the plasma periphery, a region of particular interest for driving auxiliary current. Since the bootstrap (BS) current provides a major contribution to the total current in the NSTX geometry and is driven by pitch angle diffusion across the trapped-passing boundary, this motivates study of the effect of the EBW induced scattering on the bootstrap current drive (BSCD). A simple, but sufficiently accurate, kinetic Fokker-Planck model of bootstrap-RF effects is used. The modeling results indicate that RF enhanced scattering has a small effect on the net driven current for the $\beta = 40\%$ NSTX discharge examined, at EBW powers up to 4 MW. However, significant modifications of the current drive (CD) profiles are obtained due to nonthermal pressure.

Below, the ray tracing/Fokker-Planck-quasilinear calculation of EBW current drive (EBWCD) is briefly reviewed. An approximate method for kinetic calculation of bootstrap current is demonstrated. Synergies between EBW and BS current are described for three EBW scenarios: (1) launch from a region above the equatorial midplane, which gives absorption with wave resonance in the positive toroidal current direction; (2) launch from a region symmetrically below the midplane, which gives absorption in the negative toroidal current direction; and (3) a balanced combination of the previous two scenarios.

These three scenarios will be used to sort out EBWCD-BSCD synergy effects from the simple sum of the two currents.

2. EBWCD Calculation: no synergy

For the EBW current drive modeling, the GENRAY ray tracing code [2] is used to calculate trajectories and wave *characteristics* based upon the Stix hot plasma, non-relativistic dispersion relation [3]. The wave characteristics, consisting of parallel and perpendicular wavenumbers, the wave polarizations, and the energy flux vector, are passed to the CQL3D relativistic, finite-difference, Fokker-Planck code [4]. CQL3D solves for the bounce-averaged, 2D-in-momentum-space, electron distribution on a radial array of non-circular flux surfaces.

The Fokker-Planck solution gives the balance between collisions which cause the distribution to tend towards a Maxwellian and quasi-linear diffusion which diffuses the electrons towards higher velocities. The quasi-linear calculation is relativistic, including the important relativistic mass shift on the wave-plasma resonance condition. The bounce-average in the Fokker-Planck code is over poloidal angle dependent effects on a flux surface. The resulting electron distributions are represented by $f(u, \theta, \rho)$, the distribution at the minimum magnetic field point on each flux surface. The argument u is momentum-per-rest-mass, θ is pitch angle, and ρ proportional to the square root of toroidal flux within a radial flux surface is the radial coordinate.

The trapped and transiting electron populations are fully accounted for within the bounce-averaged Fokker-Planck framework. Electron-electron collisions are self-consistent with the electron distribution, except that for purposes of obtaining the Fokker-Planck coefficients the pitch angle averaged part of the electron distribution is maintained consistent with a given temperature profile; this conserves parallel momentum in the electron-electron collisions, but enables steady-state distributions in the presence of electron heating.

The principle EBWCD effects can be illustrated by several figures derived from the codes. Figure 1 illustrates a portion of the EBW data generated with GENRAY that is passed to the CQL3D Fokker-Planck code. This is for a $I_p = 1$ MA, $B_t(0) = 0.245$ T, $\beta = 40\%$ NSTX model discharge. There is strong shifting of the parallel refractive index n_{\parallel} from injection values centered near $n_{\parallel} = 0.0$; strong n_{\parallel} -shifting is characteristic of injection of EBW off the plasma midplane [5]. n_{\parallel} -shifting is of opposite sign for injection above/below the midplane, and is mirror-symmetric about 0.0 for the up-down symmetric equilibrium used in the present study. The initial high values of n_{\perp} are in accord with launch in the EBW mode. Figure 1(f) shows absorption on Maxwellian electrons calculated from the Stix dispersion relation. Wave absorption is recalculated after coupling the ray information to the Fokker-Planck code, including relativistic effects and consistent with the resulting non-Maxwellian distributions.

The ray data passed to CQL3D, including polarizations, is tabulated at short intervals, giving many "ray elements". Each ray element within a given radial flux surface

incremental volume contributes to the summed bounce-averaged quasilinear diffusion coefficient for that volume. Figure 2 shows the resulting quasilinear diffusion coefficient ($u^2 D_{uu}$) at the radius corresponding to the peak of the EBW power absorption, $\rho = 0.64a$. The maximum momentum-per-mass, u_{norm} , on the mesh corresponds to an energy of 100 keV. Thermal velocity $v_{Te} = (T_e/m_e)^{1/2} = 0.075u_{norm}$. The parallel velocity corresponding to the Doppler-shifted third harmonic, $v_{||} = (\omega - 3\omega_{ce}/\gamma)/k_{||}$ is at positive velocity (the positive $k_{||}$ in the GENRAY code follows the convention of positiveness parallel to the vector magnetic field which in this case is in the negative toroidal direction, whereas in CQL3D positive $v_{||}$ and $k_{||}$ is in the positive, counter-clockwise, toroidal direction). Symbol γ is the relativistic factor. Also, there is a magnetic well in the plasma for high β , and the wave is approaching the third cyclotron harmonic at a frequency down-shifted from the third harmonic.

The second harmonic contribution to the diffusion is far out in the tail near the maximum negative $v_{||}$ shown in Fig. 2, and is a small effect. Within the trapping region, the diffusion coefficient is symmetrized in $v_{||}$.

It is seen that the maximum in $u^2 D_{uu}$ occurs near the trapped-passing boundary. The driven current is maximum at $\rho = 0.66a$, as shown in Fig. 3.

Figures 4 and 5 show views of the electron distribution at $\rho = 0.64a$, resulting from 1 MW of injected EBW power. From the cuts through the distribution at constant pitch angle (Fig. 4), the distribution remains near a Maxwellian up to $u = 0.27u_{norm} = 3.6v_{Te}$.

that is, Coulomb scattering dominates the EBW quasi-linear diffusion below this velocity.

The *specific* parallel current density defined as $j(u) \equiv -e \int_0^\pi d\theta u^2 \sin(\theta) u_{||} f(u, \theta, \rho)$ is shown at the top of Fig. 6, where e is the electronic charge magnitude; the bottom of Fig. 6 gives the *accumulated* current density $I(u) \equiv \int_0^u du' j(u')$. By comparison of Figs. 4 and 6, 90% of the driven EBW is occurring in the region of velocity space that is near Maxwellian.

The overall current drive efficiency from this simulation is 34.8 kA/MW. The current is in the *positive* direction, which is the direction of the equilibrium current. This corresponds to Ohkawa current [6] (OKCD) being dominant over the more familiar Fisch-Boozer current [7]. The primary effect of the EBW has been to move electrons from the parallel transiting direction into the trapped particle region, thereby creating an electron hole in the positive direction. This gives a negative electronic current, that is, a positive plasma current.

3. Bootstrap Current Calculation

3.1 Heuristic model of bootstrap current

A physical picture of bootstrap current recognizes that at each minor radius of a tokamak plasma, the density of co-current supporting trapped particles is greater than the counter-current trapped particles, assuming the usual decreasing density with radius. This result is due to the finite banana width of the particles. The co-current supporting

particles are at the outside of the banana trajectory, and have density corresponding to displacement inwards one-half a banana width. On the other hand, the counter-current supporting particles have density displaced outwards one-half a banana width. As a result, there is a *magnetization* current j_{banana} ,

$$j_{banana} = -ev_{||}(\Delta_b \frac{dn_{trap}}{d\rho}) = -\frac{\varepsilon^{3/2}}{B_{pol}} \frac{dp}{d\rho}$$

where $v_{||} = \varepsilon^{1/2}v_{Te}$, $\Delta_b = \varepsilon^{1/2}v_{Te}/\Omega_{pol}$ is the banana width, and the trapped fraction. The bootstrap current is derived from this expression and is larger by the factor $1/\varepsilon$. That is, due to pitch angle scattering the banana current acts as a source in the parallel momentum equation for the transiting electrons (and ions). For the electrons we have

$$(\frac{v_{ee}}{\varepsilon})m_e(\frac{j_{banana}}{en}) = v_{ei}m_e v_{passing},$$

that gives us an approximate relation for the bootstrap current,

$$j_{bootstrap} = -\frac{\varepsilon^{1/2}}{B_{pol}} \frac{dp}{d\rho}.$$

3.2 Simple bootstrap model applied to Fokker-Planck code

A simple bootstrap current model has been implemented in the otherwise zero-banana-width CQL3D Fokker-Planck code derived from the ideas of the previous section:

1. The calculated distribution function $f_e(u, \theta, \rho)$ is taken to be the distribution of electrons whose average radial position is ρ . The zero-banana width distribution of trapped particles calculated in the code, f_{e0} , is the zeroth order approximation to f_e .

Distribution f_{e0} is symmetric in $u_{||}$ within the trapped-particle region of velocity space.

2. To first order in banana width, the trapped particle portion of f_e at given radius ρ is

$$f_{trapped} = f_{e0}(u, \theta, \rho) - \frac{u_{||}}{\Omega_{pol}} \frac{\partial f_{e0}}{\partial \rho},$$

3. The distribution of particles is continuous at the trapped-passing boundary, including the above effect of the finite banana width.
4. To first order, the distribution of *transiting* particles f_e is equal to f_{e0} . Thus a jump, δf_{e0} , in the distribution must be added at the trapped-passing boundary to maintain continuity as in item 3:

$$\delta f_{e0} = \mp f \frac{u_{||}}{\Omega_{pol}} \frac{\partial f_{e0}}{\partial \rho}$$

To implement this jump within the Fokker-Planck code, it was only necessary to adjust all references to f_{e0} at the trapped-passing boundary, looking from the passing-particle region by the jump δf_{e0} . This algorithm change was done *explicitly-in-time*, that is, using values from the previous time step. The code has otherwise fully-implicit differentials. This amount of explicitness did not noticeably destabilize the differencing. For the NSTX case being examined in this report, the plasma current is positive (counter-clockwise looking from above). The jump δf_{e0} is negative at the positive $u_{||}$ trapped-passing boundary, and positive at the negative $u_{||}$ boundary. This reduces the distribution

for positive direction transiting particles and increases it in the opposite direction, giving the bootstrap current.

Electron bootstrap current density calculated with the adjusted Fokker-Planck code is compared with the bootstrap current from a standard model by Sauter *et al.* [8], in Figure 7. Application of the standard bootstrap model in the present case includes using the NSTX magnetic geometry to calculate the effective trapped fraction of electrons. We see that there is excellent agreement between the approximate CQL3D model and the standard model, for $\rho/a > 0.4$. The value $\rho/a = 0.4$ corresponds to inverse aspect ratio $\varepsilon \equiv (R_{max} - R_{min})/(R_{max} + R_{min}) = 0.21$. Beyond this value of ε , the simple trapped-passing model in CQL3D is evidently accurate.

Figure 8 shows the specific parallel bootstrap current density versus velocity u . It peaks at $u/u_{norm} = 0.19$ ($u/v_{Te} = 2.5$), and the cumulative parallel current is at 90% of its full value at $u/u_{norm} = 0.275$ ($u/v_{Te} = 3.7$). Thus, the bootstrap current mainly involves electrons within the Maxwellian portion of the EBW heated distribution in Fig. 4.

The bootstrap model can also simulate radial diffusion within the neoclassical banana regime. A Ware pinch term would also need to be implemented in order to obtain steady state density profiles. However, the present modeling is simplified by holding the density profiles constant.

Westerhof and Peters [9] have incorporated additional refinements to the above bootstrap current model in a 2D Fokker-Planck code, and compare their augmented model results with those obtained using their version of the above simple bootstrap model. In Ref. [9], the jump condition at the trapped-passing boundary is augmented to account for the fact that particles that pitch angle scatter from the trapped region to transiting do not jump the full half-banana width in radius: the transiting particles near the trapped-passing boundary also undergo a finite excursion from their orbit-averaged radial flux surface. This effect reduces the bootstrap current from that obtained by the simple trapped-passing jump-condition approximation. Good agreement is obtained between the refined bootstrap current calculation and the standard results of Sauter *et al.* [4] over the full range of ϵ . Westerhof and Peters find that their refined calculation leads to less than 10% reduction of the calculated bootstrap current compared to the simple jump-condition model for $\epsilon > 0.2$ in the case of ∇T_e -induced bootstrap current, and for $\epsilon > 0.1$ in the case of ∇n_e -induced bootstrap current. The reduction of bootstrap current relative to the approximate bootstrap calculation increases to about 50% at $\epsilon = 0.005$. These results agree with the results of the present calculation, shown in Fig. 7. We conclude that the jump-condition approach to bootstrap current is accurate to within $\sim 10\%$ for the outer 60% of the NSTX discharge radius.

4. EBW and BS Synergy

We report results of combining the bootstrap current model in CQL3D as described above, with RF diffusion due to EBW. Three scenarios are considered: (1) injection of

EBW such that OKCD is generated in support of the equilibrium plasma current as in section 2, above; (2) wave injection with reversed $n_{//}$, obtained by injection of the waves from below the equatorial plane; and (3) symmetric injection, combining equal powers of waves injected as in the the above two cases. Three injection powers have been studied: 0.1, 1.0, and 4.0 MW. The objective of the three injection scenarios is to sort out possible synergy effects.

Physical considerations lead to the result that the additional bootstrap current *due to RF pitch angle scattering* will be increased in the positive current direction regardless of the direction of the resonance velocity of the waves. Waves with positive resonance velocity increase the propagation of the negative jump δf_{e0} from the trapped-passing boundary into the co-transiting region, and negative resonance velocity waves propagate a positive increase of the distribution into the counter-transiting region. In both cases, the bootstrap current is increased. On the other hand, modification of the plasma pressure profile will give additional bootstrap current in proportion to the local $(-\nabla n)$ -profile.

Summary results are presented in three tables. The *RF+synergy BS current*, that is, the RF current including RF effects on the bootstrap current, is obtained by subtracting the pure BS current from the combined RF+BS current. This RF+synergy BS current can be compared with RF-only current to separate out the effects of the RF pitch angle scattering. In Table 1, for 0.1 MW RF power, the RF+synergy BS current is a few percent *less* than the RF current in the absence of the bootstrap effect. The net current arising from synergy between EBW and BS current drive is small and negative. This is

counter intuitive. However, as the RF power increases, positive additional bootstrap current ~ 10 kA is obtained for all three $n_{||}$ -scenarios. The net increase in bootstrap current due to synergy is not large, 11% at 4.0 MW RF power. However, there is a significant effect on the radial profile of the driven current.

More details on these results will be given in order to discern: (1) why the net synergy effect on the current is small, (2) why, at low power, the synergy between the RF and bootstrap current *reduces* the net RF current.

Table 2 and 3 provide further summary results to help discern the underlying physics. Reversing the $n_{||}$ in the spectra, Table 2, reverses the RF current drive and, at low power, the contribution of synergy to the RF current. In Table 3, results for balanced spectra show very small net synergy current. [The SS in the table refers to the single sided (in $n_{||}$) spectra driven current.]

The combined EBWCD and BS current profiles, and the average electron energy density versus plasma radius, for the case of 1.0 MW with EBWCD adding to the equilibrium current, are shown in figures 9 and 10. This is the same RF co-current case as for Fig. 3, but with the BSCD model turned on. Although the energy has a local maximum near $\rho = 0.64a$, the net plasma current density (opposite to the electron current) is not driven negative by the bootstrap component. This is due to the positive contribution of the EBWCD shown in Fig. 3.

Figure 11 shows a decomposition of the driven currents: [solid line] EBW+Synergy BS is the (EBWCD+BSCD, Fig. 9) minus the BSCD, Fig. 6; [dashed line] is simple EBWCD, Fig. 3; [dash-dot line] is EBW+Synergy BS minus the separate contributions of the EBWCD, Fig. 3, and the BSCD, Fig. 6. The additional synergy current (dash-dot line) appears simply to be bootstrap current from the modified energy profile in Fig. 10. Thus, the RF pitch angle scattering would produce a symmetric enhancement of the BSCD. But BSCD from the locally enhanced energy (pressure) profile produces BSCD that is anti-symmetric about the RF interaction region.

Figure 12 shows the same data as Fig. 11, except EBW power is 0.1 MW. The 0.1 MW case shows very small deviation of the average energy profile from the background profile. In this case, there is very little current beyond the driven EBWCD.

At up to 1 MW applied EBW power, it is evident that the EBWCD strongly dominates any possible enhancement of the BSCD due to pitch-angle scattering. The pitch-angle scattering effect is expected to give a simple enhancement of the BSCD. The synergy contribution in Figs. 11 and 12 appear anti-symmetric around the RF power deposition region, indicating rather that the synergy current is simply due to the modification of the energy profile. Westerhof and Peters [10] arrived at a similar conclusion for ECCD scenarios in the RTP and DIII-D tokamaks.

Figure 13 shows results for the 1 MW symmetric EBW spectra. The solid curve shows the additional BS current due to the application of the EBW power. The average

energy profile is very close to Fig. 11. The resulting additional BS current to the EBW power is close to identical in the two cases of single-sided n_{\parallel} -spectra (Fig. 12, dash-dot line) and symmetric spectra (Fig. 13, solid line). This further verifies that, up to 1 MW, there is no significant bootstrap current due to the additional pitch angle scattering by the RF wave. Also, from Table 3, additional bootstrap current due to the RF enhanced scattering is small (<10% of the single-sided- n_{\parallel} EBWCD). Evidently, the collisional scattering dominates the RF scattering, even at 1 MW RF power. This is also clear from Figs 4, 6, and 7, in that the distribution is near Maxwellian throughout most of the velocity space region where the RF current is driven. That is, at up to 1 MW input power, pitch angle scattering due to collisions is dominant over the RF pitch angle scattering in the region of velocity space important for BS current production.

At the 4 MW input power level, the effect of additional RF pitch angle scattering begins to become important. This is clear from the Table 1-3 results, which show a positive contribution of the RF to bootstrap current regardless of the direction of the n_{\parallel} -spectra.

Figure 14 shows the current density profile for 4 MW of EBW injected with symmetric n_{\parallel} -spectra. There is negligible EBWCD in this case, when the bootstrap effect is not included. The primary effect of the localized EBW heating is to produce a nonthermal electron tail giving a local average energy of the electrons about equal to the that at the center of the discharge. This produces an anti-symmetric negative and positive bootstrap current density approximately proportional to localized increase in plasma

pressure gradient. The amplitude of the additional current density ($\sim \pm 45 \text{ A/cm}^2$) is comparable to the peak single-sided EBWCD current density for 4 MW ($\sim 55 \text{ A/cm}^2$). The EBW induced pitch angle scattering gives greater width to the positive portion of the localized RF induced bootstrap current, resulting in the 10.48 kA of synergy current in Table 3. Radial transport effects may greatly reduce the effect described in this paragraph. Future studies will address this.

There is a question of why the synergetic bootstrap current, for example in the case of symmetric spectra, is negative in the low power cases. There is a slight reduction in co-current traveling electrons and increase in counter-current electrons, which gives the bootstrap current. We conjecture that this asymmetry could reduce the Ohkawa CD slightly in the co-current direction and increase it in the opposite direction, giving negative synergy current.

5. Discussion and Conclusions

A simple kinetic bootstrap current model in the CQL3D Fokker-Planck code is shown to give accurate results at $\rho > 0.4a$ for a $\beta = 40\%$ NSTX target discharge. Modeling the additional bootstrap current obtained which arises due to application to 1 MW of EBW power, absorbed in a localized region near the plasma periphery ($\rho = 0.65a$) shows that the BS current is primarily due to increased non-Maxwellian plasma pressure induced by the EBW power, although the precise amount may be different than obtained from Maxwellian-based neoclassical formulae. Any additional bootstrap current due to

the RF induced scattering appears to be relatively small at this power level, consistent with the observation that the RF does not cause significant quasi-linear distortion of the electron distribution in the main region of velocity space where the bootstrap current is generated.

At 4 MW of applied RF power, there is evidently a synergistic increase in the bootstrap current due to enhanced RF pitch angle scattering of the electrons. The synergistic contribution to the net current is a 10% effect.

The creation of localized nonthermal electron pressure causes localized bootstrap current that is comparable to driven EBWCD. Driving counter-current outside of a neoclassical tearing mode island would reinforce the stabilizing effect of driving co-current within the island. However, the effects of radial transport on this phenomena will be a subject of future studies.

The effect of radial particle transport induced by the Ohkawa CD has not been included in our calculations. In a fully neoclassical plasma, this transport would lead to a change in the plasma density profile and consequent modified bootstrap current which would cancel the Ohkawa current drive, consistent with conservation of canonical toroidal angular momentum [11, 12]. The net effect would be a smaller Fisch-Boozer current drive, reduced by trapping effects, that is opposite to the Ohkawa current drive. However, plasmas have much greater electron radial transport than the neoclassical values. Experiments aimed at accurate measurement of Ohkawa current drive will be directly

addressing physics issues of radial particle transport and conservation of canonical toroidal angular momentum.

Acknowledgments

Dr. Michel McCoy (LLNL) constructed the core CQL3D code, including the bootstrap coding. Dr. Ken Kupfer (Bayer Corporation) added mathematical rationale for the simple bootstrap model used in this code. Drs. R.J. Goldson (PPPL) and N.J. Fisch (PPPL) encouraged this work. The work is supported under U.S. Department of Energy grant DE-FG03-02ER54684 and contract DE-AC02-76CH03073.

References

- [1] G. Taylor, P.C. Efthimion, C.E. Kessel, R.W. Harvey, A.P. Smirnov, N.M. Ershov, M.D. Carter, and C.B. Forest, *Phys. of Plasmas* **11**, 4733 (2004).
- [2] A.P. Smirnov and R.W. Harvey, "The GENRAY Ray Tracing Code", CompX report CompX-2000-01 (2001); "Calculations of the Current Drive in DIII-D with the GENRAY Ray Tracing Code", *Bull. Amer. Phys. Soc.* **40**, 1837, Abstract 8P35 (1995).
- [3] T.H. Stix, *Waves in Plasmas*, AIP (1992).
- [4] R.W. Harvey and M.G. McCoy, "The CQL3D Fokker-Planck Code", *Proc. of IAEA Technical Committee Meeting on Advances in Simulation and Modeling of Thermonuclear Plasmas*, Montreal, 1992, p. 489-526, IAEA, Vienna (1993) [available through USDOC/NTIS, document DE93002962].
- [5] C.B. Forest, P.K. Chattopadhyay, R.W. Harvey, and A.P. Smirnov, *Phys. of Plasmas* **7**, 1352 (2000).
- [6] T. Ohkawa, "Steady state operation of tokamaks by RF heating", GA Report GA-A13847 (1976), available from USDOC/NTIS, document PB2000-108008.
- [7] N.J. Fisch and A.H. Boozer, *Phys. Rev. Lett.* **45**, 720 (1980).
- [8] O. Sauter, C. Angioni, and Y.R. Lin-Liu, *Phys. of Plasmas* **6**, 2834 (1999).
- [9] E. Westerhof and A.G. Peters, *Computer Phys. Comm.* **95**, 131 (1996).
- [10] E. Westerhof and A.G. Peters, "Fokker-Planck code calculations on neoclassical transport in strongly nonthermal plasmas", Poster at 5th European Fusion Theory Conf., El Excorial, Madrid, Spain (1993).

- [11] N.J. Fisch, Rev. Modern Phys. **59**, 175 (1987).
- [12] R.W. Harvey and R.O. Dendy, Phys. Fluids **B4**, 902 (1992).

Figure Captions

Figure 1

EBW ray trajectories and characteristics: (a) rays projected in the poloidal plan; (b) zooming on rays; (c) top view of trajectories; (d) $n_{//}$ versus distance in poloidal plan showing rapid upshift for off-midplane launch; (e) n_{\perp} versus poloidal distance; and (f) power flowing in each ray (ergs/sec) versus ω_{ce}/ω showing wave launch with frequency slightly above the second harmonic, and absorption primarily as the third harmonic is approached.

Figure 2

RF quasi-linear $u^2 D_{uu}$ -diffusion coefficient in the radial bin centered at $\rho = 0.64a$. The coefficient is mostly due to the third harmonic interactions, but a second harmonic contribution is shown in the region $u_{//}/u_{norm} = -0.75$ to -1.0 . The contours begin at 1/2 the peak value, and decrease by factor 1/2 at each successive contour.

Figure 3

Driven EBW current density versus radius in 1 MW co-current case.

Figure 4

Cuts versus u through the distribution at constant pitch angles, corresponding to perpendicular direction, trapped-passing boundary, parallel and anti-parallel directions in momentum space. Plasma radius is $\rho = 0.64a$. Injected power is 1 MW. The distribution is substantially non-Maxwellian above $3.6v_{Te} = 0.27u_{norm}$.

Figure 5

Contours of the electron distribution shown in Fig. 4. Contour values are chosen to give constant spacing for a Maxwellian.

Figure 6

(a) Specific current density $j(u)$ versus u in top figure, and (b) accumulated current

$I(u) \equiv \int_0^u du' j(u')$. Ninety percent of the net current is driven in the velocity space region which is near-Maxwellian, i.e., below $3.6v_{Te}$.

Figure 7

Comparison of electron bootstrap current calculated with simple model (dashed line) with banana regime result of Sauter *et al.* [4] analysis (dash-dot line). The calculations agree well beyond $\rho = 0.4$.

Figure 8

Specific parallel bootstrap current versus u , and cumulative parallel current resulting from bootstrap current model, evaluated at radius $\rho = 0.64a$. This is a bootstrap current only calculation.

Figure 9

Driven current profile due to combined EBW and bootstrap effect. Conditions are otherwise the same as in Fig. 3. RF power is 1 MW.

Figure 10

Average electron energy versus radius. The 1 MW of EBW power creates a local maximum in average energy.

Figure 11

EBWCD plus synergy BS (solid), EBWCD (dashed), and synergy bootstrap (dotted) currents, for the 1 MW co-current EBW power.

Figure 12

Same curves as for Fig. 11, except these are for EBW power 0.1 MW.

Figure 13

Symmetric EBW spectra: 1 MW: EBW plus BS (solid), EBWCD (dashed), for 1 MW of EBW power.

Figure 14

Current density profile for 4 MW symmetric n_{\parallel} -spectra.

Case	RF Power (MW)	Net Current (kA)	Comment
BS only	-	496.106	
RF only, no BS	0.1	4.141	0.59-0.72a. peak@0.64 a
RF+BS	0.1	500.079	RF peak@0.64 a
RF+Synergy BS	0.1	3.97	(RF+BS)-(BS only), -4.2% RF
RF only	1.0	34.790	RF peak: 0.64 a
RF+BS	1.0	530.370	RF peak: 0.64 a
RF+Synergy BS	1.0	34.26	(RF+BS)-(BS only), -1.5%
RF only	4.0	100.95	
RF+BS	4.0	608.23	
RF+Synergy BS	4.0	112.12	(RF+BS)-(BS only), 11.0% RF

Table 1: EBWCD supporting equilibrium current

Case	RF Power (MW)	Net Current (kA)	Comment
BS only	-	496.106	
RF only, no BS	0.1	-4.157	0.59-0.72a. peak@0.64 a
RF+BS	0.1	491.786	RF peak@0.64 a
RF+Synergy BS	0.1	-4.320	(RF+BS)-(BS only), +4% RF
RF only	1.0	-34.887	RF peak: 0.64 a
RF+BS	1.0	460.743	RF peak: 0.64 a
RF+Synergy BS	1.0	-35.363	(RF+BS)-(BS only), +1.4%
RF only	4.0	-100.968	
RF+BS	4.0	405.128	
RF+Synergy BS	4.0	-90.978	(RF+BS)-(BS only), -9.0% RF

Table 2: EBWCD counter to equilibrium current

Case	RF Power (MW)	Net Current (kA)	Comment
BS only	-	496.106	
RF only, no BS	0.1	-0.009	Good cancellation
RF+BS	0.1	495.932	
RF+Synergy BS	0.1	-0.373	(RF+BS)-(BS only), small syn
RF only	1.0	-0.077	
RF+BS	1.0	495.382	
RF+Synergy BS	1.0	-2.581	(RF+BS)-(BS only), 7.4% SS RF
RF only	4.0	0.200	
RF+BS	4.0	506.583	
RF+Synergy BS	4.0	10.48	(RF+BS)-(BS only), 10.4% SS RF

Table 3: Symmetric wave spectra in co-/counter-current direction

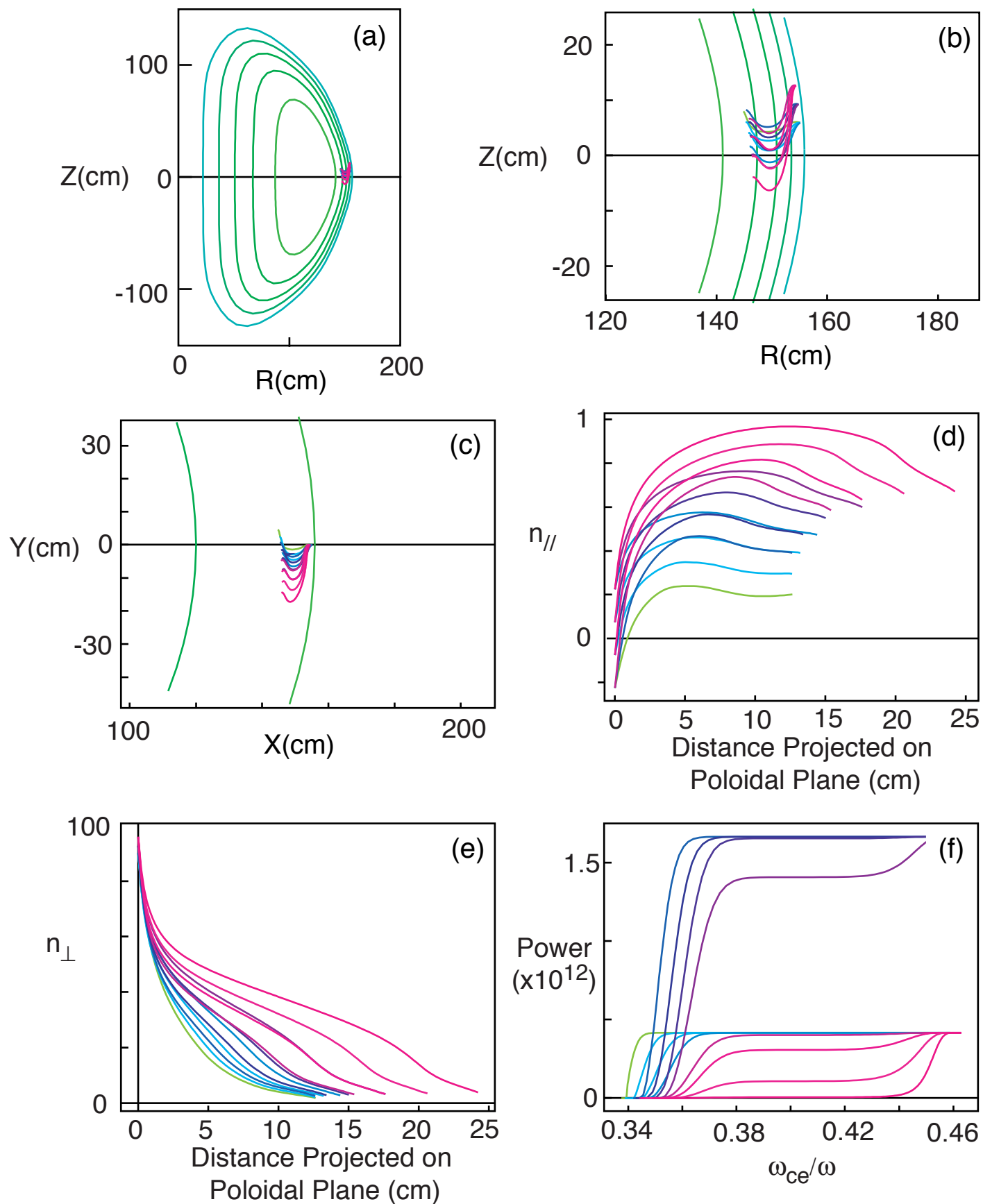


Figure 1

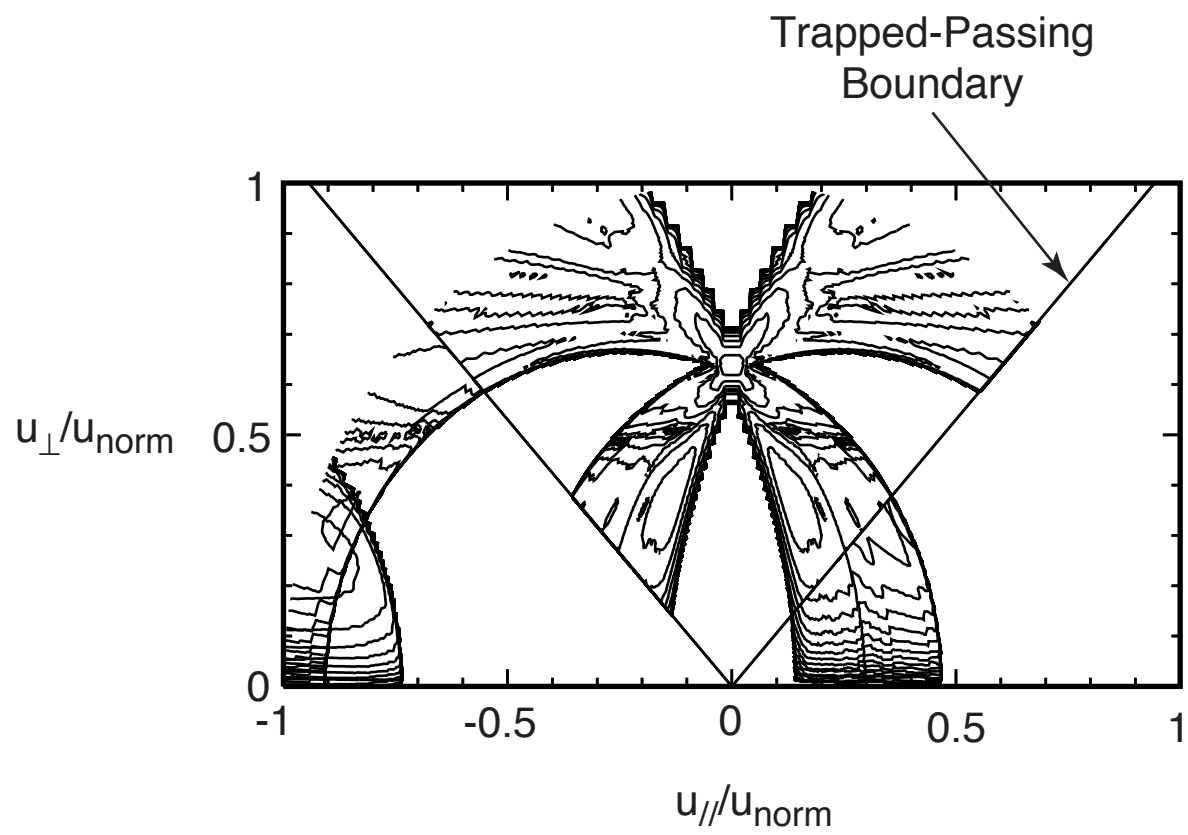


Figure 2

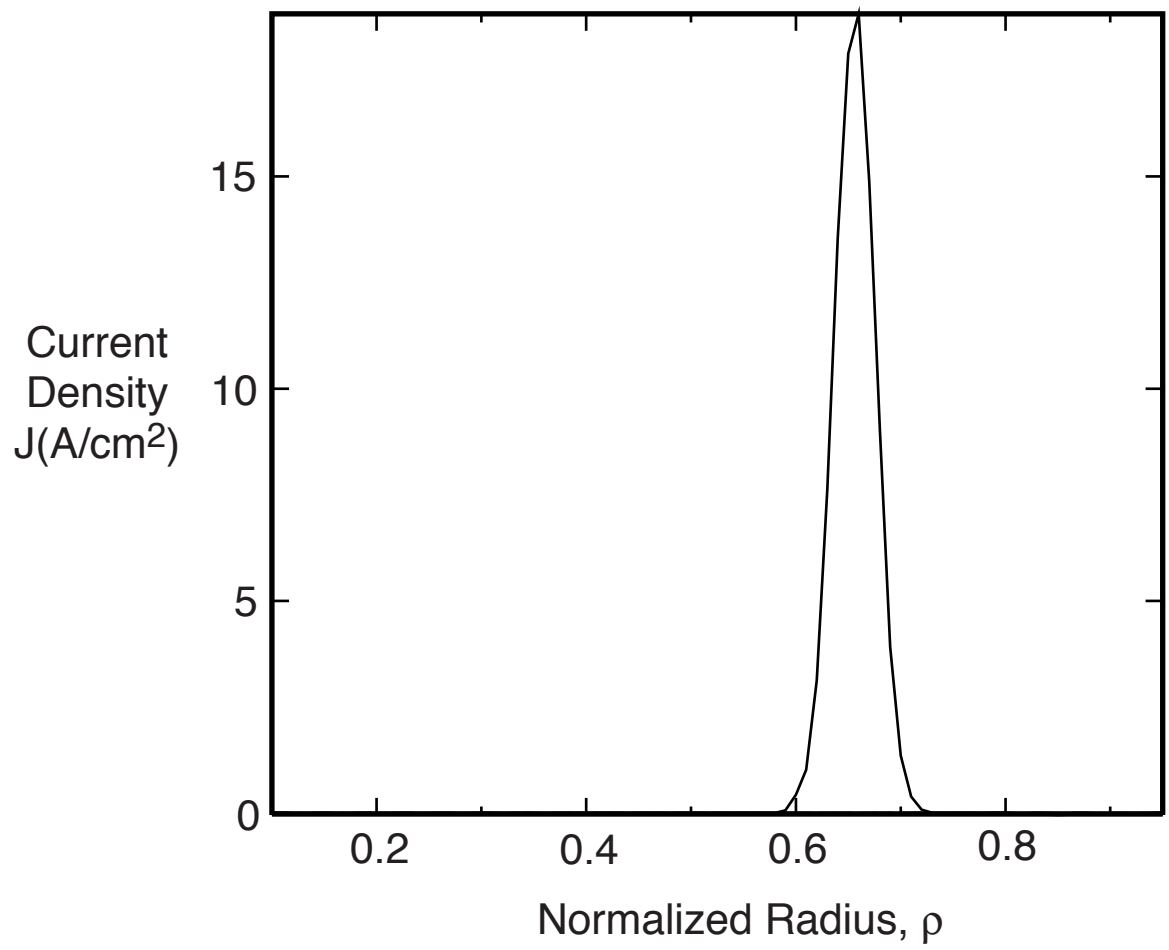


Figure 3

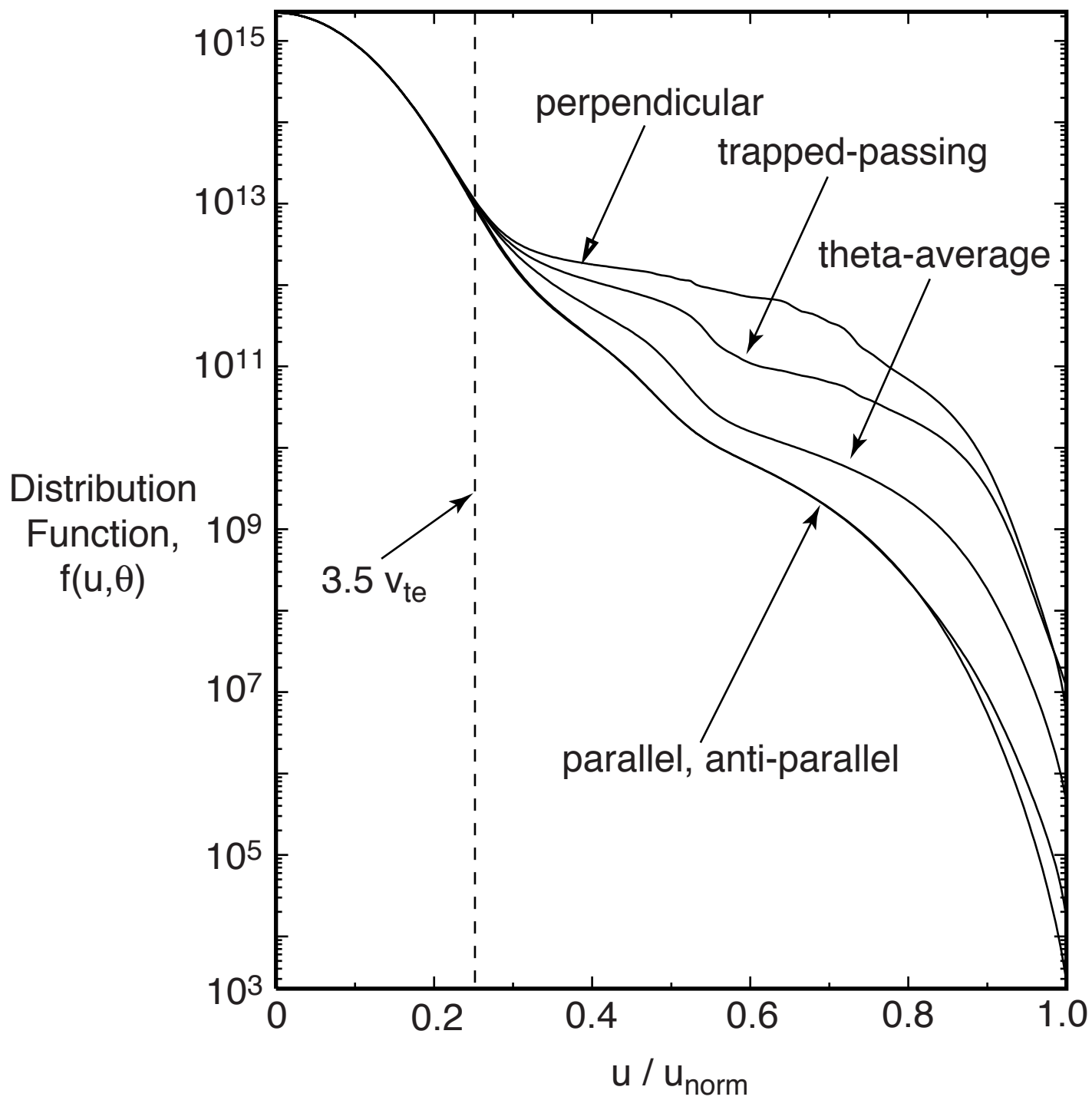


Figure 4

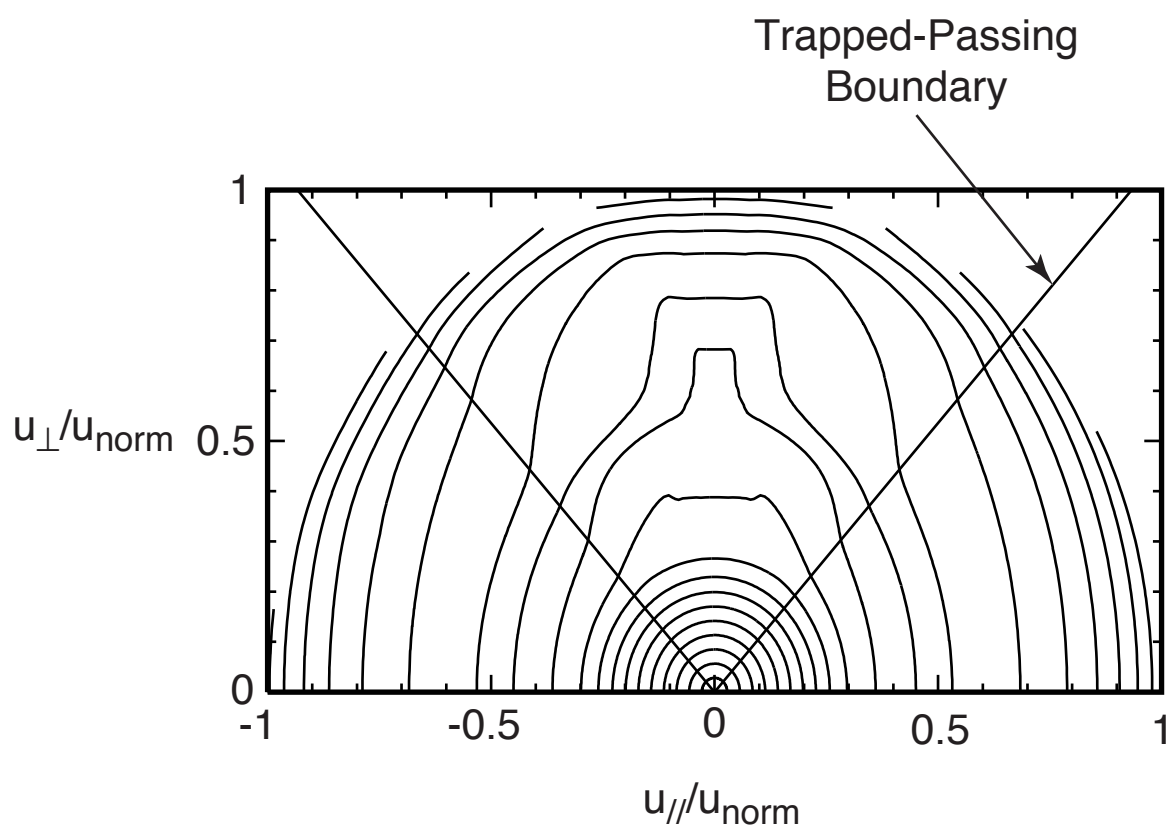


Figure 5

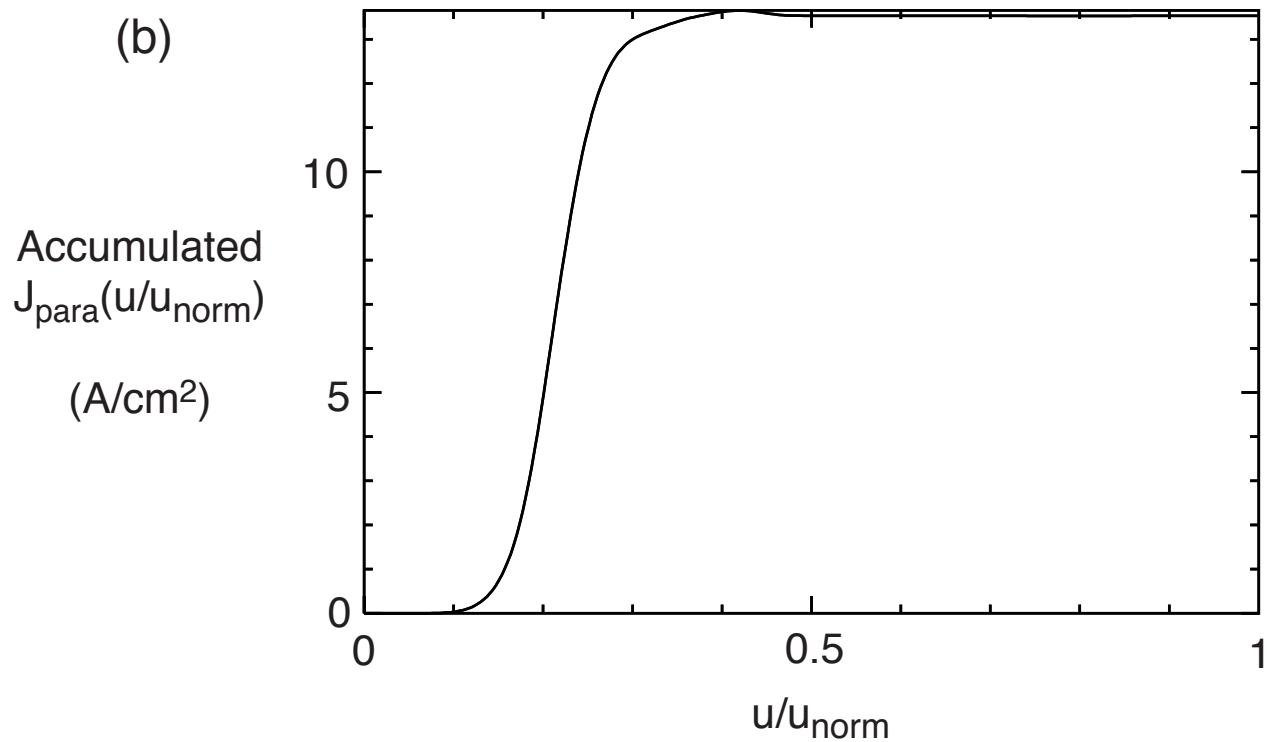
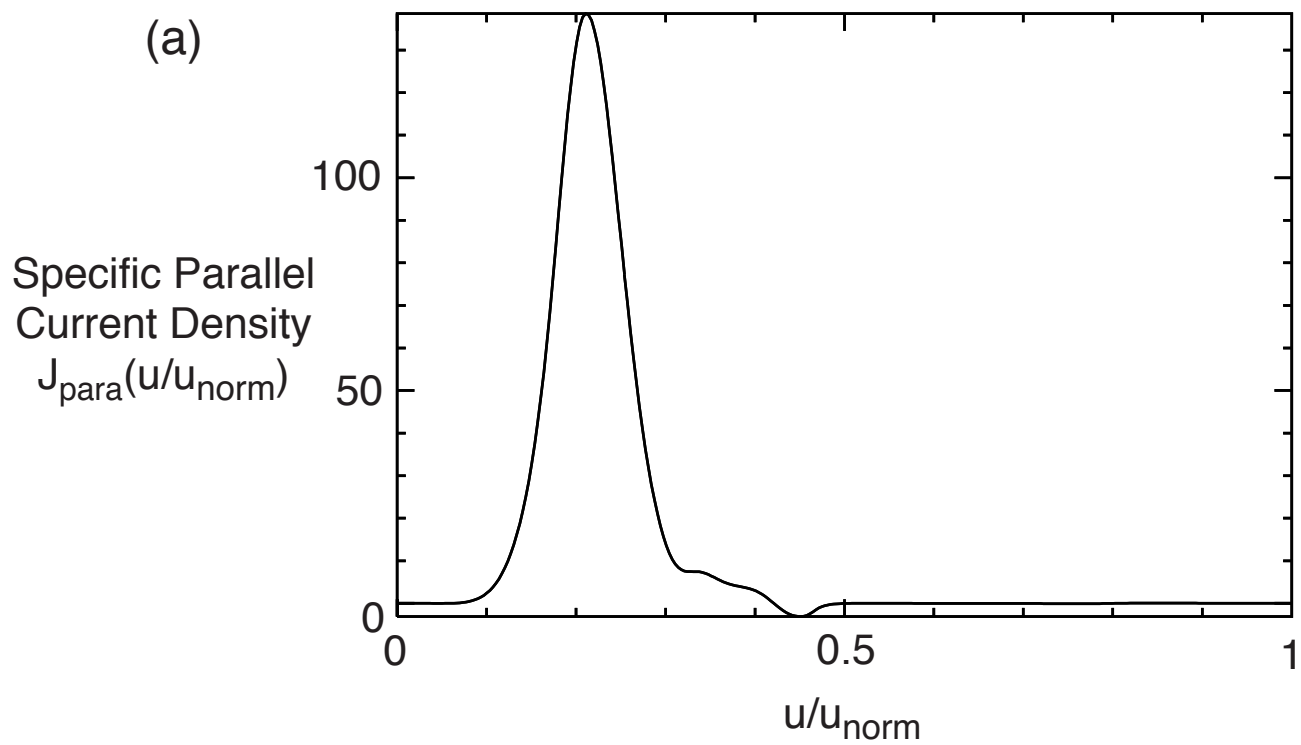


Figure 6

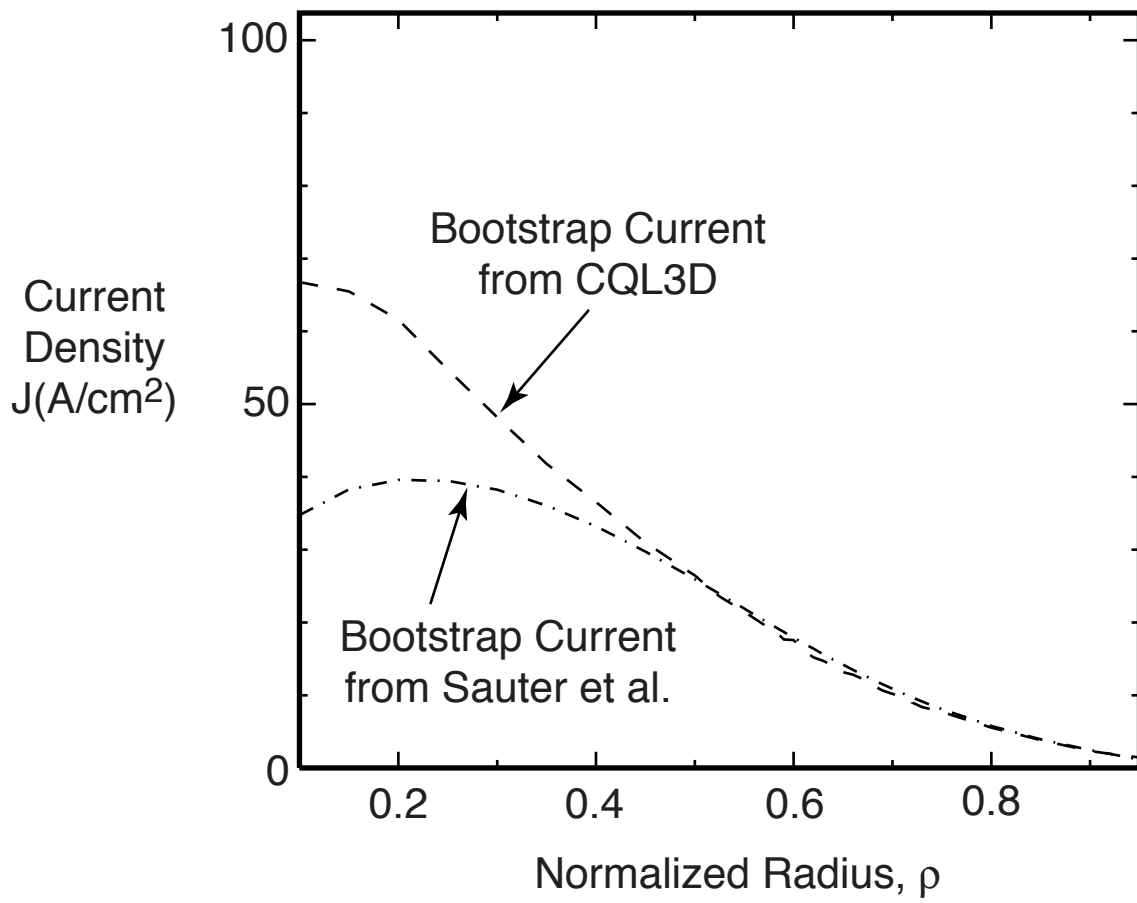


Figure 7

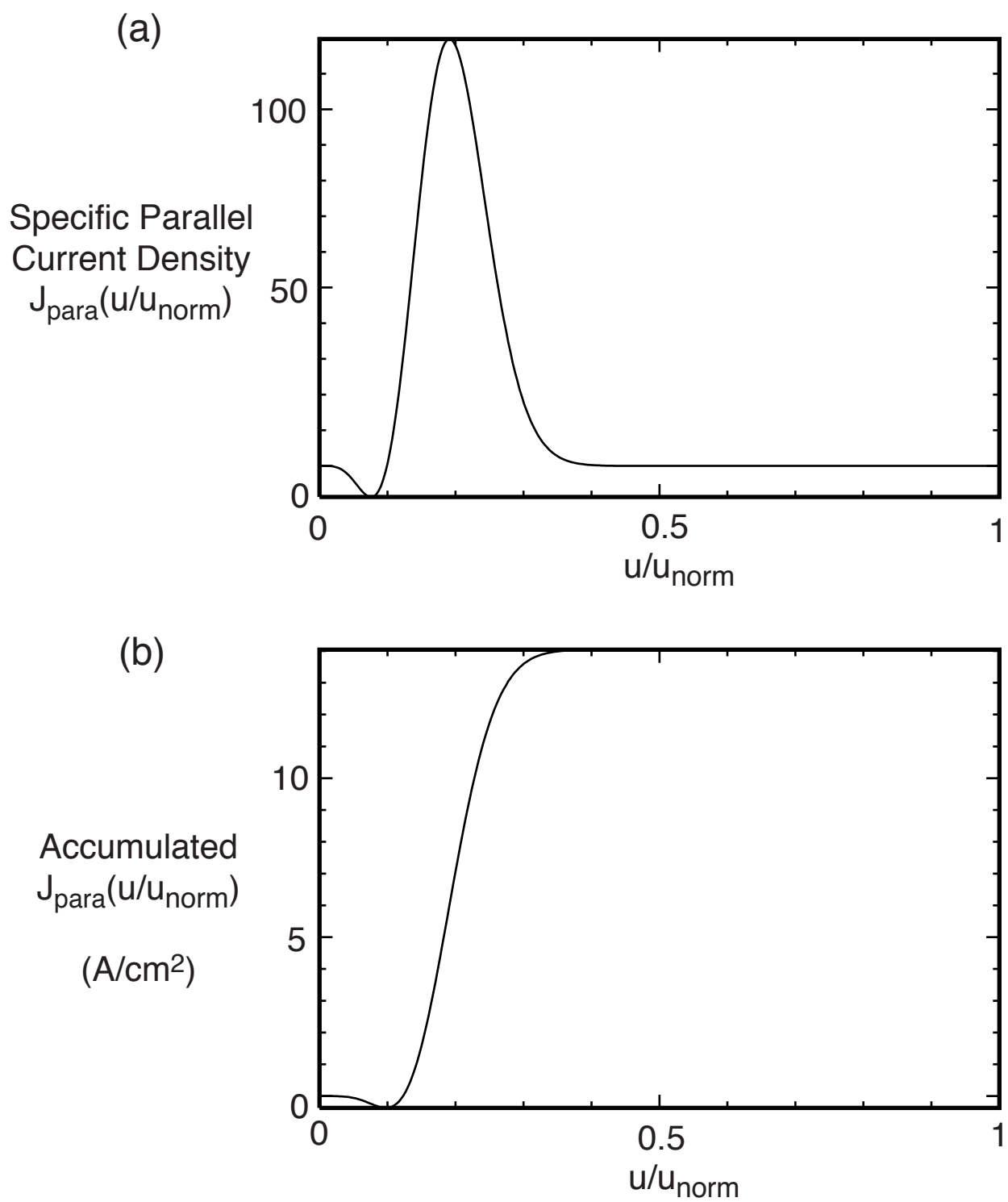


Figure 8

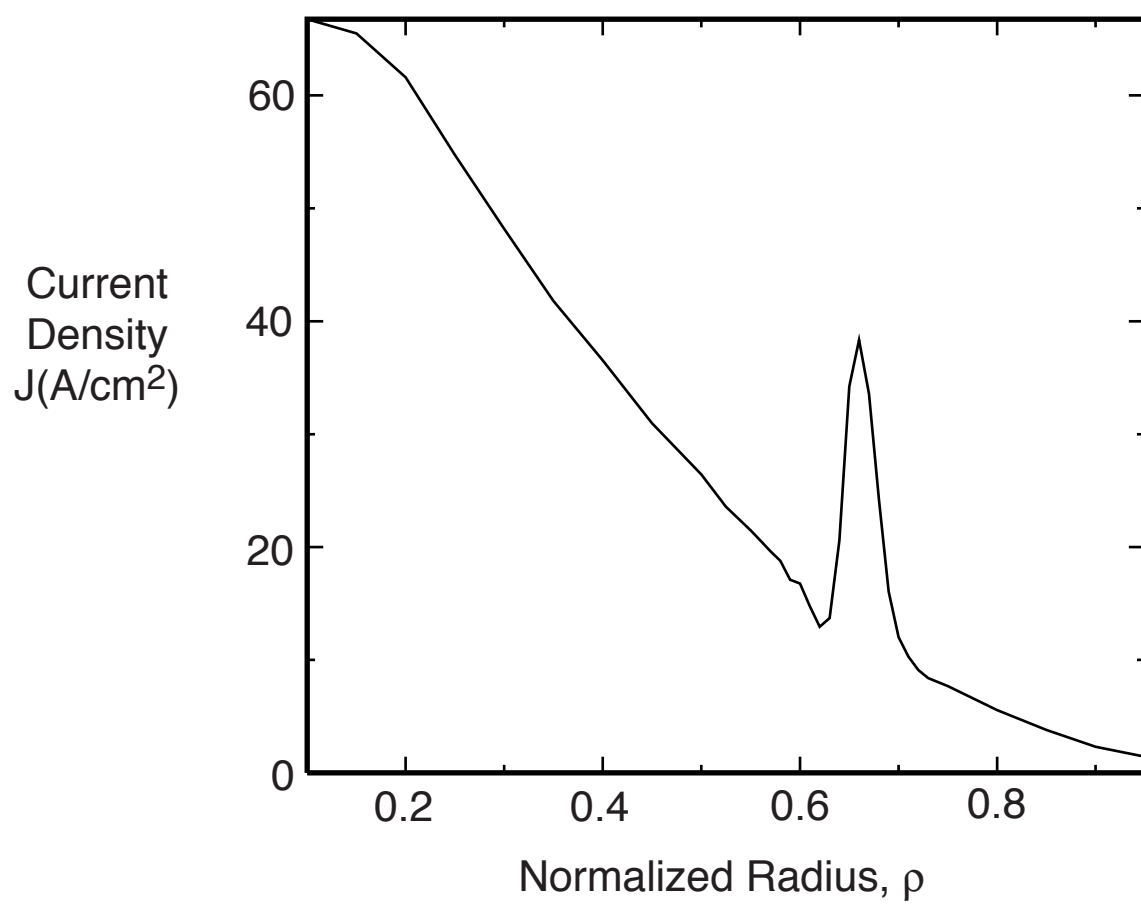


Figure 9

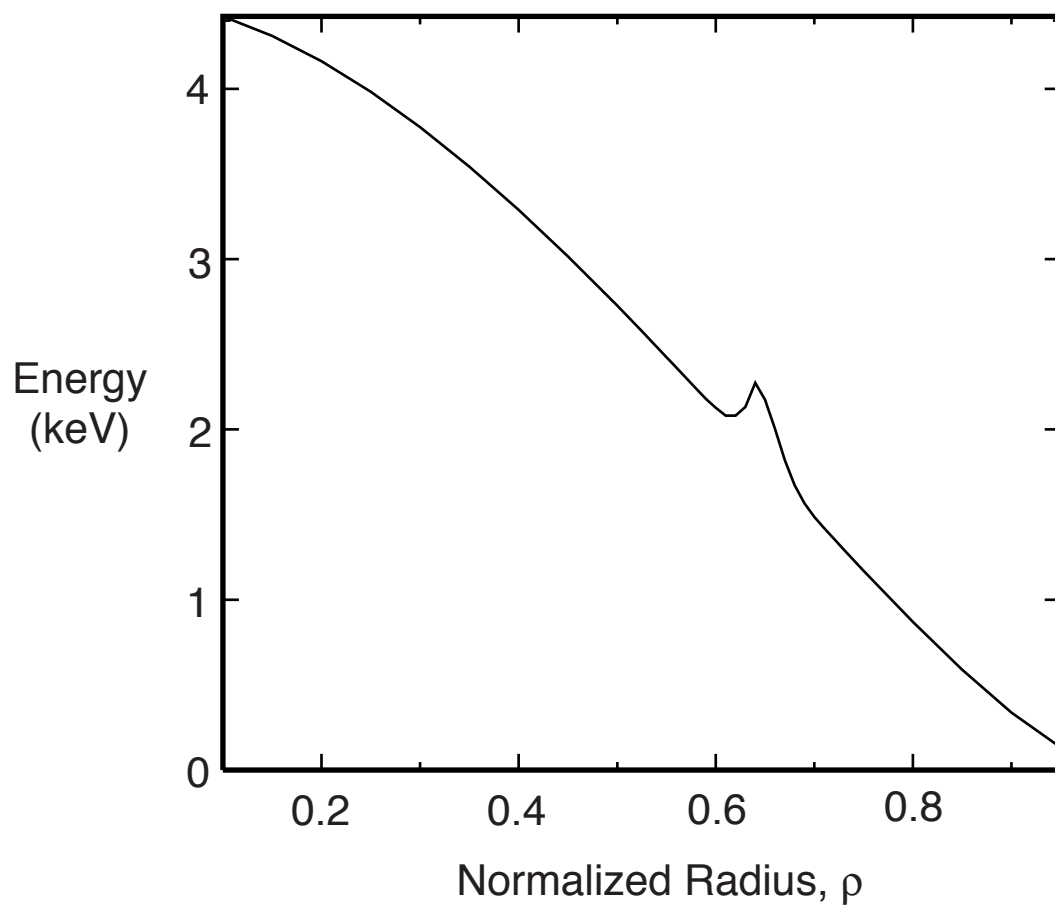


Figure 10

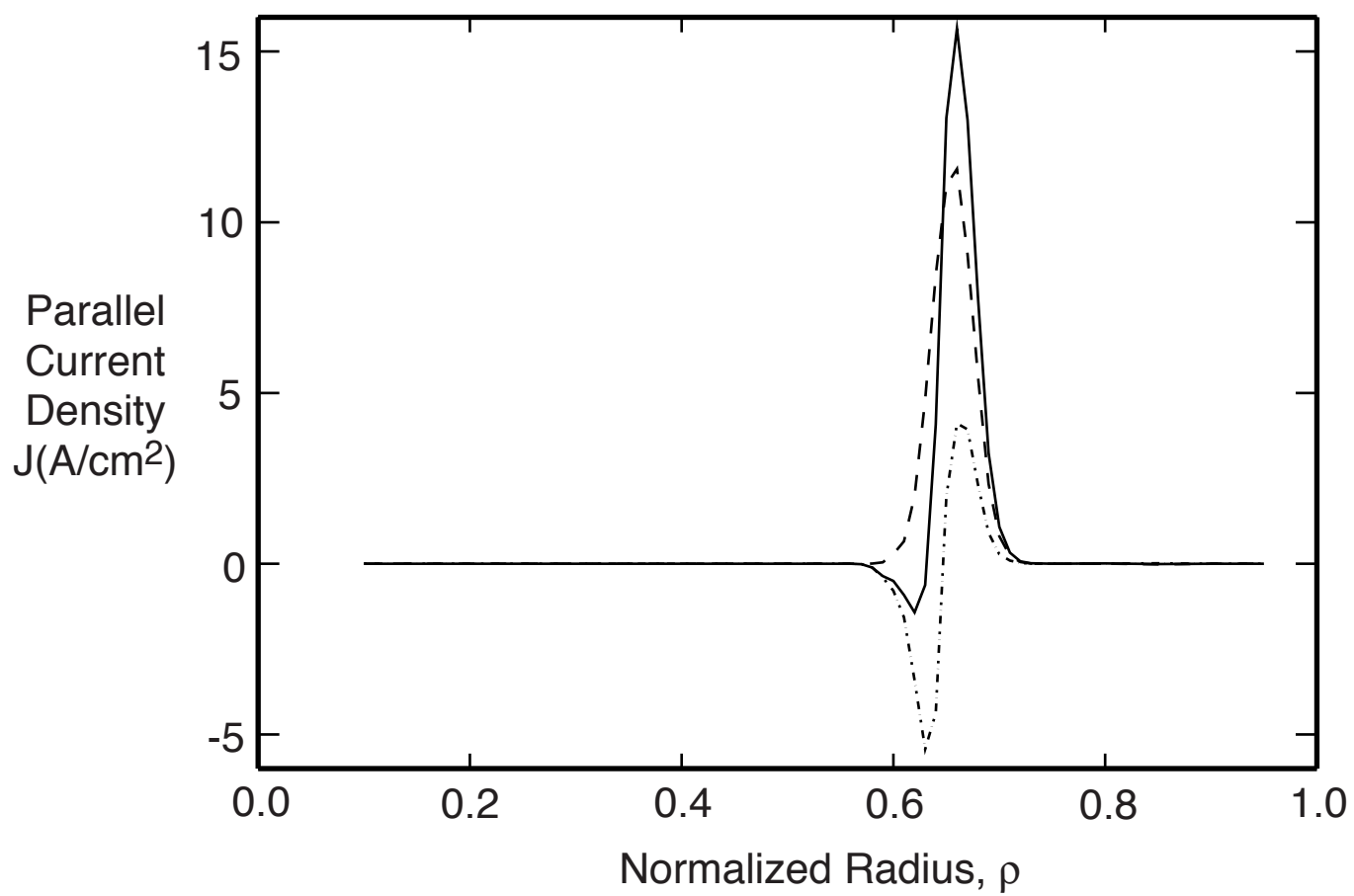


Figure 11

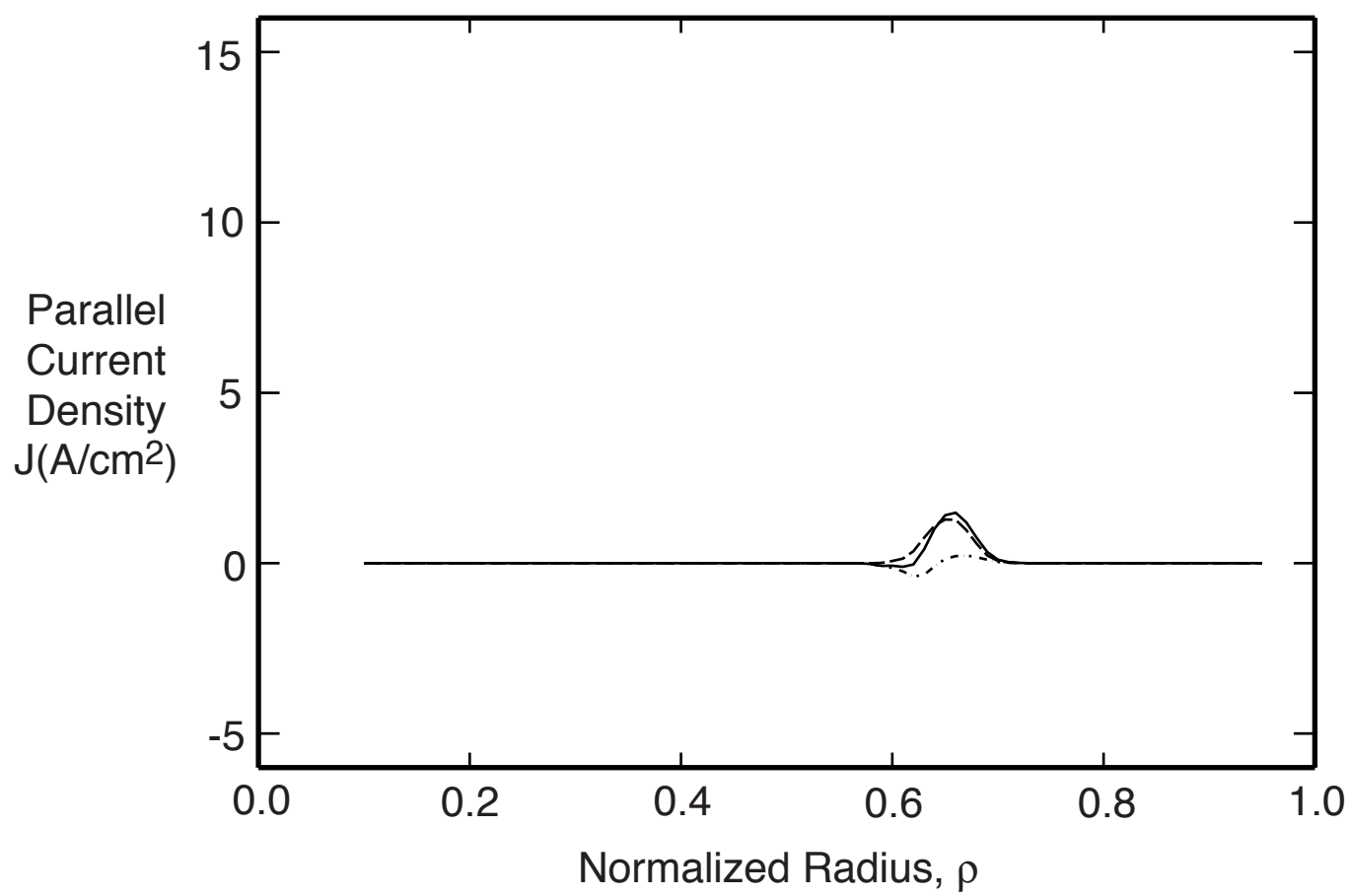


Figure 12

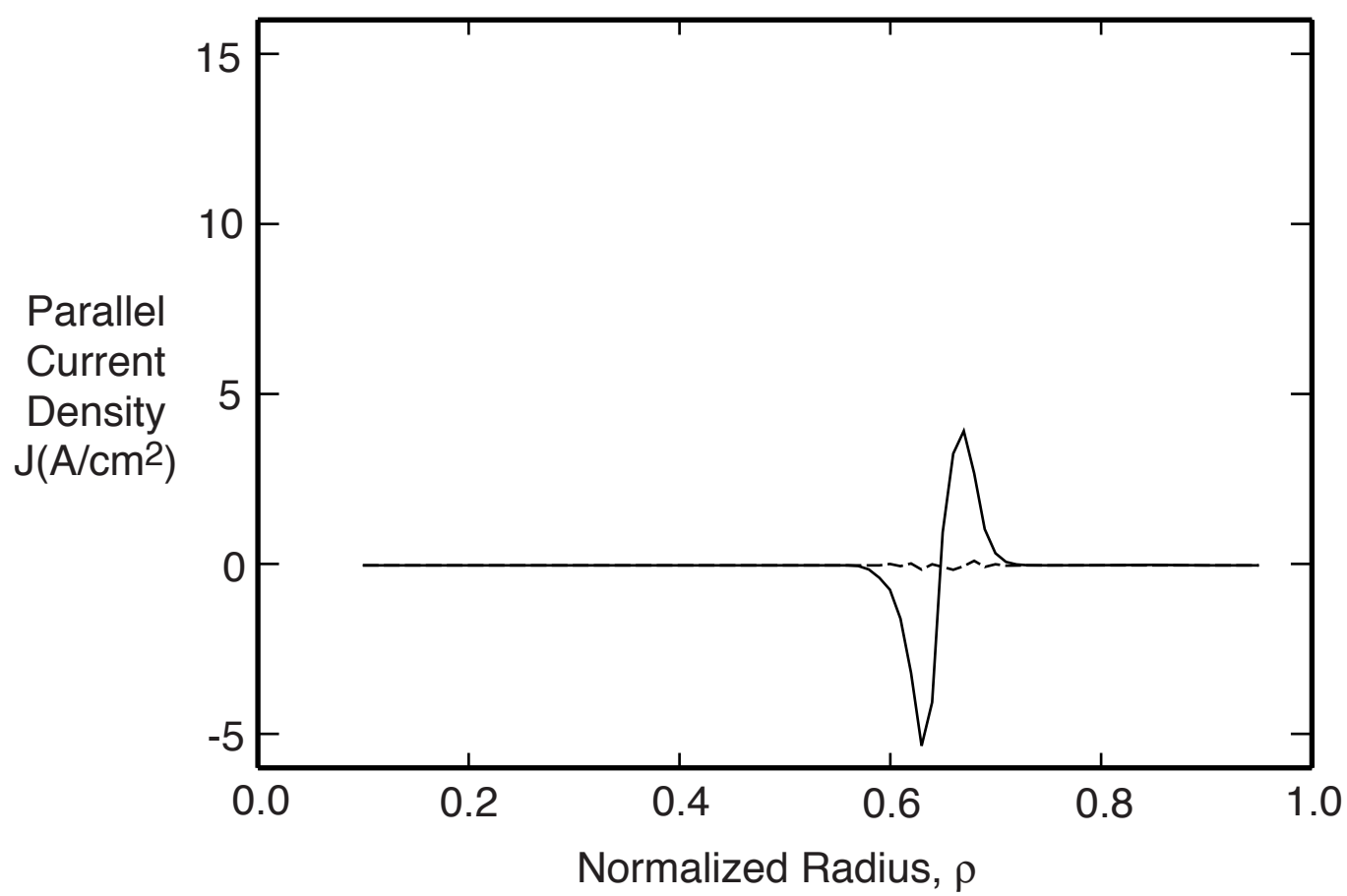


Figure 13

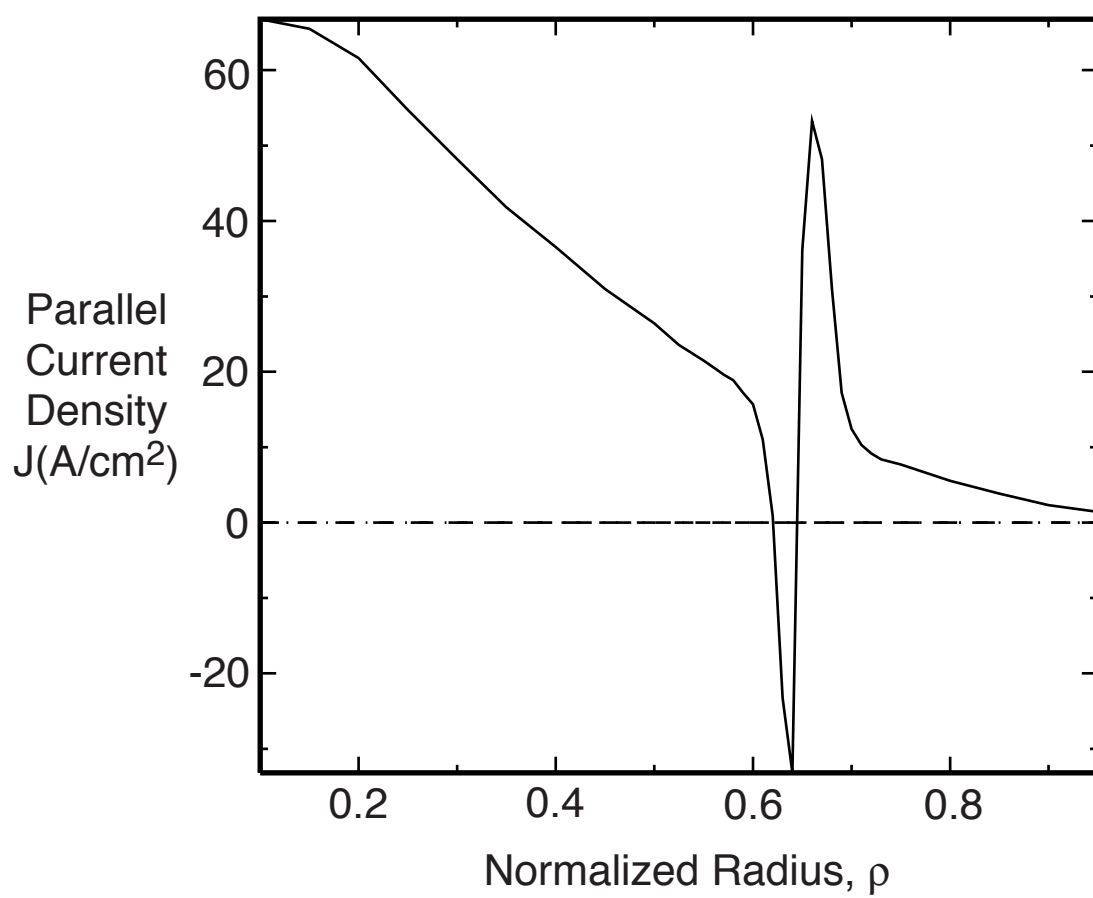


Figure 14

External Distribution

Plasma Research Laboratory, Australian National University, Australia
Professor I.R. Jones, Flinders University, Australia
Professor João Canalle, Instituto de Fisica DEQ/IF - UERJ, Brazil
Mr. Gerson O. Ludwig, Instituto Nacional de Pesquisas, Brazil
Dr. P.H. Sakanaka, Instituto Fisica, Brazil
The Librarian, Culham Science Center, England
Mrs. S.A. Hutchinson, JET Library, England
Professor M.N. Bussac, Ecole Polytechnique, France
Librarian, Max-Planck-Institut für Plasmaphysik, Germany
Jolan Moldvai, Reports Library, Hungarian Academy of Sciences, Central Research Institute
for Physics, Hungary
Dr. P. Kaw, Institute for Plasma Research, India
Ms. P.J. Pathak, Librarian, Institute for Plasma Research, India
Professor Sami Cuperman, Plasma Physics Group, Tel Aviv University, Israel
Ms. Clelia De Palo, Associazione EURATOM-ENEA, Italy
Dr. G. Grosso, Instituto di Fisica del Plasma, Italy
Librarian, Naka Fusion Research Establishment, JAERI, Japan
Library, Laboratory for Complex Energy Processes, Institute for Advanced Study,
Kyoto University, Japan
Research Information Center, National Institute for Fusion Science, Japan
Dr. O. Mitarai, Kyushu Tokai University, Japan
Dr. Jiangang Li, Institute of Plasma Physics, Chinese Academy of Sciences,
People's Republic of China
Professor Yuping Huo, School of Physical Science and Technology, People's Republic of China
Library, Academia Sinica, Institute of Plasma Physics, People's Republic of China
Librarian, Institute of Physics, Chinese Academy of Sciences, People's Republic of China
Dr. S. Mirnov, TRINITI, Troitsk, Russian Federation, Russia
Dr. V.S. Strelkov, Kurchatov Institute, Russian Federation, Russia
Professor Peter Lukac, Katedra Fyziky Plazmy MFF UK, Mlynska dolina F-2,
Komenskeho Univerzita, SK-842 15 Bratislava, Slovakia
Dr. G.S. Lee, Korea Basic Science Institute, South Korea
Dr. Rasulkhozha S. Sharafiddinov, Theoretical Physics Division, Institute of Nuclear Physics,
Uzbekistan
Institute for Plasma Research, University of Maryland, USA
Librarian, Fusion Energy Division, Oak Ridge National Laboratory, USA
Librarian, Institute of Fusion Studies, University of Texas, USA
Librarian, Magnetic Fusion Program, Lawrence Livermore National Laboratory, USA
Library, General Atomics, USA
Plasma Physics Group, Fusion Energy Research Program, University of California
at San Diego, USA
Plasma Physics Library, Columbia University, USA
Alkesh Punjabi, Center for Fusion Research and Training, Hampton University, USA
Dr. W.M. Stacey, Fusion Research Center, Georgia Institute of Technology, USA
Dr. John Willis, U.S. Department of Energy, Office of Fusion Energy Sciences, USA
Mr. Paul H. Wright, Indianapolis, Indiana, USA

The Princeton Plasma Physics Laboratory is operated
by Princeton University under contract
with the U.S. Department of Energy.

Information Services
Princeton Plasma Physics Laboratory
P.O. Box 451
Princeton, NJ 08543

Phone: 609-243-2750
Fax: 609-243-2751
e-mail: pppl_info@pppl.gov
Internet Address: <http://www.pppl.gov>